Mass cytometry deep phenotyping of human mononuclear phagocytes and myeloid-derived suppressor cells from human blood and bone marrow

Mikael Roussel, P. Brent Ferrell, Allison R. Greenplate, Faustine Lhomme, Simon Le Gallou, Kirsten E. Diggins, Douglas B. Johnson, Jonathan M. Irish

Mass cytometry deep phenotyping of human mononuclear phagocytes and myeloid derived suppressor cells from human blood and bone marrow

Mikael Roussel,[*,†,‡,§,1] P. Brent Ferrell, Jr.,[¶] Allison R. Greenplate,[*] Faustine Lhomme,[‡] Simon Le Gallou,[‡,§] Kirsten E. Diggins,[†] Douglas B. Johnson,[¶] and Jonathan M. Irish[*,†,1]

[*]Department of Pathology, Microbiology and Immunology, Vanderbilt University School of Medicine, Nashville, TN, USA
[†]Department of Cancer Biology and Vanderbilt-Ingram Cancer Center, Vanderbilt University School of Medicine, Nashville, TN, USA
[‡]CHU de Rennes, Pole de Biologie, Rennes, France
[§]INSERM, Unité Mixte de Recherche U1236, Université Rennes 1, Etablissement Français du Sang Bretagne, Equipe Labellisée Ligue Contre le Cancer, Rennes, France
[¶]Department of Medicine, Vanderbilt University, Nashville, TN, USA

Summary sentence: Single cell mass cytometry of human mononuclear phagocyte cells reveals myeloid phenotypes and highlights S100A9 as a key MDSC marker

Short title: CyTOF delineates mononuclear system

[1]**Correspondence:** Mikael Roussel, Laboratoire d'Hématologie, CHU Pontchaillou, 2 rue Henri Le Guilloux, F-35033 Rennes, France, Phone: +33 (0) 299 289 142, E-mail: mikael.roussel@chu-rennes.fr and Jonathan M. Irish, Vanderbilt University School of Medicine, 740B Preston Building, 2220 Pierce Avenue, Nashville, TN 37232-6840, USA; Phone: +1 (615) 875 0965; E-mail: jonathan.irish@vanderbilt.edu

Keywords: CyTOF, MDSCs, macrophages, monocyte

Character count: 22,884 characters
Number of figures: 6 figures (6 in color)
Number of references: 67
Abstract word count: 249 words
Summary sentence word count: 20

Abbreviations
CyTOF = cytometry by time-of-flight
DC = dendritic cell
GM-CSF = granulocyte-macrophage colony-stimulating factor
HD = healthy donor
IFN□ = interferon gamma
IL-10 = interleukin 10
IL-4 = interleukin 4
LPS = lipopolysaccharide
M-CSF = macrophage colony-stimulating factor
MDSC = myeloid-derived suppressor cell
MEM = marker enrichment modeling
MPS = monocyte phagocyte system
PBMC = peripheral blood mononuclear cell
SPADE = spanning-tree progression analysis of density-normalized events
TNF□ = tumor necrosis factor
TPP = TNF□ Pam3 PGE2
viSNE = visualization of t-distributed stochastic neighbor embedding

Abstract

The monocyte phagocyte system (MPS) includes numerous monocyte, macrophage, and dendritic cell (DC) populations that are heterogeneous both phenotypically and functionally. In this study, we sought to characterize these diverse MPS phenotypes with mass cytometry (CyTOF). To identify a deep phenotype of monocytes, macrophages, and dendritic cells, a panel was designed to measure 38 identity-, activation-, and polarization- markers including CD14, CD16, HLA-DR, CD163, CD206, CD33, CD36, CD32, CD64, CD13, CD11b, CD11c, CD86, and CD274. MPS diversity was characterized for (1) circulating monocytes from healthy donors, (2) monocyte-derived macrophages further polarized *in vitro* (i.e. M-CSF, GM-CSF, IL-4, IL10, IFNγ, or LPS long-term stimulations), (3) monocyte-derived DCs, and (4) myeloid-derived suppressor cells (MDSCs), generated *in vitro* from bone marrow and/or peripheral blood. Known monocyte subsets were detected in peripheral blood to validate the panel and analysis pipeline. Then, by using various culture conditions and stimuli before CyTOF analysis, a multidimensional framework for the MPS compartment was constructed and registered against historical M1- or M2- macrophages, monocyte subsets, and DCs. Notably, MDSCs generated *in vitro* from bone marrow expressed more S100A9 than when generated from peripheral blood. Finally, to test the approach *in vivo*, peripheral blood from melanoma patients (n = 5) was characterized and observed to be enriched for MDSCs with a phenotype of $CD14^{pos}HLA\text{-}DR^{low}S100A9^{high}$ (3% of PBMC in healthy donors, 15.5% in melanoma patients, $p < 0.02$). In summary, mass cytometry comprehensively characterized phenotypes of human monocyte, MDSC, macrophage, and DC subpopulations in both *in vitro* models and patients.

Introduction

The monocyte phagocyte system (MPS) is a complex cellular compartment that includes phenotypically and functionally heterogeneous cells, including monocyte, macrophage, and dendritic cells (DC) populations [1]. MPS cells belong to the innate immune system, whose activities can include infection defense, tissue homeostasis and controlling T cell immunity [2-4].

Phenotypic definition of myeloid cells is variable because of the lack of consistency between markers first identified in mice and humans. For example, while macrophages and myeloid-derived suppressor cells (MDSCs) are typically defined as $F4/80^{high}$ and $Gr1^{pos}$ respectively in mice [5], in humans EMR1 (the human F4/80 homolog) is expressed on eosinophils instead of macrophages [6], and Gr1 has no human homolog [7]. Furthermore, there are few unique marker of cell identity, as most of the markers of interest (e.g. CD14, CD11b, CD33, HLA-DR, CD64) are shared by various myeloid cells and none is lineage-specific. Finally, myeloid cells, particularly monocytes and macrophages, are highly plastic with respect to phenotype and function and depend upon various surrounding signals for differentiation/polarization. In the context of cancer or sepsis, an altered myelopoiesis can give rise to suppressive myeloid cells with poor phagocytic activity [8]. Overall, this complexity of phenotype is highlighted by the growing literature on monocyte, DC, or macrophage nomenclature [1,8-11]. In particular, monocytes are classified in 4 phenotypic subsets ($CD14^{pos}CD16^{neg}$, $CD14^{pos}CD16^{pos}$, $CD14^{dim}CD16^{pos}Slan^{low}$, and $CD14^{dim}CD16^{pos}Slan^{high}$) [10,12], however, within these traditional phenotypes, additional functional subsets have been discovered, such as Tie2-expressing monocytes (TEMs), involved in angiogenesis, or monocytic-MDSCs, involved in T-

cell immune suppression [8,13]. Moreover, the paradigm of macrophage polarization has dramatically evolved in the last decade from a binary polarization (classically-activated [M1, IFNγ- or LPS- driven] vs. alternatively-activated [M2, IL4- or IL10-driven]) to a much more complicated landscape [11,14,15]. Recently, Xue and colleagues assessed the transcriptional landscape of multiple activated human macrophage subpopulations generated by numerous *in vitro* stimuli [16]. At least nine clusters were found to recapitulate macrophage polarization status, in particular an already described regulatory macrophage (M_TPP) associated with tumor necrosis factor (TNF), prostaglandin E2 and TLR2-ligand stimuli [16-18].

At the protein level, characterization of these heterogeneous cell types has been largely accomplished with "low resolution" approaches (e.g., morphological evaluation and immunohistochemistry), wherein only one or a few proteins were used to identify populations, as an example, CD68 and CD163 are frequently proposed to characterize macrophage types [19]. High-resolution approaches such as mass cytometry (also known as cytometry by time-of-flight, or CyTOF) are valuable in order to better understand their diversity, function and identify potential targets for novel therapies [2,15,20]. CyTOF combined with high-dimensional analysis, in particular visualization of t-distributed stochastic neighbor embedding (viSNE), spanning-tree progression analysis of density-normalized events (SPADE), and marker enrichment modeling (MEM), are robust methods to identify numerous and novel subsets from heterogeneous populations [21-26]. Indeed, several studies using CyTOF have explored the immune compartment including B-, T-, NK-, or myeloid cells either from peripheral blood or from tissues [21,27-38]. In particular, Becher and colleagues developed a myeloid dedicated panel to characterize myeloid cells across eight mice

tissues, which revealed previously unidentified populations in mice tissues using an unsupervised approach of CyTOF data [29,39].

We hypothesized that human MPS complexity would benefit from a high-dimensional single cell approach [20,39,40]. Here, a single mass cytometry panel comprised of 38 antibodies was combined with high dimensional analysis methods with the aim of deciphering the human MPS compartment in primary samples including peripheral blood mononuclear cells (PBMCs) from healthy donors and from patients with melanoma. Results from primary cells were compared to observations from *in vitro* models of myeloid differentiation using human blood and bone marrow cells exposed to established polarizing inflammation factors. Unsupervised analysis tools, including viSNE, SPADE, and MEM, were used to create and describe a comprehensive reference framework for the MPS compartment and to characterize an abnormal abundance of MDSCs in the peripheral blood of melanoma patients.

Materials and Methods

Samples and mononuclear cells preparation

Peripheral blood from healthy donors (HDs) or from melanoma patients was obtained in accordance with the Declaration of Helsinki following protocols approved by Vanderbilt University Medical Center (VUMC) Institutional Review Board. Bone marrow from HDs was obtained under French legal guidelines and fulfilled the requirements of the University Hospital of Rennes institutional ethics committee. Peripheral blood was drawn by venipuncture into heparinized tubes. Bone marrow was obtained by aspiration after sternotomy for cardiac surgery and cells were kept in sodium heparin bags. Mononuclear cells were isolated using Ficoll-Paque PLUS (GE Healthcare Bio-sciences, Uppsala, Sweden) centrifugation. Freshly isolated mononuclear cells were immediately cryopreserved in FBS (Life Technologies, Grand Island, NY, USA) containing 12% DMSO (Fischer Scientific, Fair Lawn, NJ, USA). For *in vitro* monocyte-derived cells experiments, buffy coats from HDs were obtained according to protocols accepted by the institutional review board at the university hospital from Rennes. After collection, monocytes were purified from PBMC by elutriation before cryopreservation (plate-forme DTC, CIC Biotherapie 0503, Nantes, France). Monocytes represented more than 85% of the cells.

In vitro culture and stimulation

For *in vitro* differentiations, cells were cultured in 6-wells plates at $2x10^6$ cells/mL in a humidified atmosphere at 37°C, 5% CO2 in RPMI 1640 (Mediatech Inc, Manassas, VA) enriched with FCS 10% (Gibco, Life technologies) and supplemented with 1% PenStrep solution (Gibco, Life technologies). MDSCs were derived from

peripheral blood- or bone marrow- mononuclear cells. Cells were cultured for 4 days and activations were performed with GM-CSF (40 ng/mL; Peprotech, Rocky Hill, NJ) and G-CSF (40 ng/mL; Peprotech) and, for bone marrow cells, GM-CSF and IL-6 (40 ng/mL; Peprotech) as previously described [41,42]. Immature DCs were generated from monocytes by GM-CSF and IL-4 (40 ng/mL; EMD Millipore, Billerica, MA) for 6 days, media were changed at 3 days. Then for terminal differentiation, TNFα (10 ng/mL; EMD Millipore) was added in culture for 2 days. Macrophage at baseline (M_b) was generated from monocytes by stimulation by M-CSF (50 ng/mL; Cell Signaling, Danvers, MA) for 3 days, as previously described [16]. Then M_b were further polarized during 3 days, by IL-4, IL-10 (10 ng/mL; Peprotech), IL-6 (10 ng/mL; Peprotech), IFNg (10 ng/mL; Cell Signalling), LPS (10 ng/mL; Sigma-Aldrich, St Louis, MO), or TPP (TNFα [10 ng/mL; EMD Millipore]; Pam3CSK4 [100 ng/mL; Invivogen, San Diego, CA]; prostaglandine E2 [1 μg/mL, Sigma]). At the end of each condition culture, except for DCs, wells were treated with Accutase (Sigma Aldrich) prewarmed at 37°C, for 30 sec, before collection, washing and staining.

Allogeneic three-way Mixed Lymphocyte Reaction assay

Suppressive capacities of *in vitro* PBMC- and bone marrow- derived MDSCs were determined in an allogeneic three-way mixed lymphocyte reaction (MLR) assay. T cells were purified from PBMCs from a healthy donor using the Pan T Cell isolation kit (Miltenyi Biotec, Bergisch Gladbach, Germany). DCs and MDSCs were obtained by culture conditions described above. DCs were derived from PBMCs obtained from an allogeneic donor. MDSCs were obtained from 3 donors for PBMCs and 2 for bone marrows. After 4 days of *in vitro* differentiation, $CD14^{pos}CD33^{pos}CD11b^{pos}HLA\text{-}DR^{low}$ MDSC from bone marrow and monocytes were sorted using a FACS ARIA cell sorter

(BD Biosciences). For MLRs reaction, 1 x 10^5 T cells of one donor were seeded in culture media with 2,000 allogeneic DCs and different MDSC:T ratio (1:8, 1:4, 1:2). The MLR assays were carried out during 5 days in round-bottomed 96-well plates to ensure efficient DC/T cell contact. T cell proliferation was measured by thymidine uptaking (1 µCi/well) during the last 16 h.

Antibodies, cell labeling and mass cytometry analysis

Purified antibodies from Biolegend (San Diego, CA, USA) or Immunotech (Marseille, France) were labeled using MaxPar DN3 labeling kits (Fluidigm, San Francisco, CA), titrated and stored at 4°C in antibody stabilization buffer (Candor Bioscience GmbH, Wangen, Germany). Antibodies from Miltenyi Biotech (Bergisch Gladbach, Germany) or R&D systems (Minneapolis, MN) were labeled with FITC, PE or APC (Table S1). Antibodies metal-tagged were from Fluidigm. Cell labeling and mass cytometry analysis was performed as previously described [20,43]. Briefly, cells were incubated with a viability reagent (cisplatin, 25 µM; Enzo Life Sciences, Farmingdale, NY, USA) as previously described [44]. Then, 3x10^6 cells were washed in phosphate buffered saline (PBS, HyClone Laboratories, Logan, UT) containing 1% bovine serum albumin (BSA, Fisher Scientific, Fair Lawn, NJ) and stained in 50 µL PBS and BSA 1% containing antibody cocktail. Cells were stained for 30 minutes at room temperature using antibodies listed (Table S1). Cells were washed twice in PBS and BSA 1% and then fixed with 1.6% paraformaldehyde (PFA, Electron Microscopy Sciences, Hatfield, PA, USA). Cells were washed once in PBS and permeabilized by resuspending in ice cold methanol. After incubating overnight at -20°C, cells were washed twice with PBS and BSA 1% and stained with iridium DNA intercalator (Fluidigm) for 20 minutes at room temperature. Finally, cells were

washed twice with PBS and twice with diH_2O before being resuspended in 1x EQTM Four Element Calibration Beads (Fluidigm) and collected on a CyTOF 1.0 mass cytometer (Fluidigm) at the Vanderbilt Flow Cytometry Shared Resource. Events were normalized as previously described [45].

Data processing and analysis

Data analysis was performed using the workflow already described [46]. Raw median intensity values were transformed to a hyperbolic arcsine (arcsinh) scale with a cofactor of 5. Analysis was performed on Cytobank using published techniques including SPADE, viSNE and hierarchical clustering [25,47]. Each file was pre-gated on singlets and viable cells as defined by cisplatin and iridium gating. The analysis pipeline was as follows: after gating on nucleated cells ($Iridium^{pos}$), the labeling was assessed on biaxial plots on $CD45^{pos}$ cells. Then, a viSNE analysis was performed. On the viSNE map, B-, T-, and NK- cells were distinguished, and then the remaining cells were engulfed in a MPS gate, and were further clustered with SPADE. Heat maps were performed using the marker enrichment modeling (MEM) algorithm [24].

Statistical analysis

Statistical analyses were performed with GraphPad Prism 5.0 software (GraphPad Software, San Diego, CA, USA) using Wilcoxon or Mann-Whitney tests as appropriate.

Results

CyTOF delineates four monocyte subsets in peripheral blood from HDs

In order to recapitulate the diversity and heterogeneity of monocyte subsets, a CyTOF panel using 38 parameters was designed (Table S1). Based on literature profiling, proteins in this panel were expected to be expressed at different levels for MPS cell types and associate with differentiation, polarization, and activation states. PBMCs from HDs were first tested and the MPS gate defined with the analysis pipeline (Figure 1A, B, and S1A). To characterize known and expected monocyte sub-populations in peripheral blood (*i.e.* classical, intermediate, and non-classical), the analysis was initially defined to seek 30 nodes representing populations of phenotypically distinct cells. In manual review of the features distinguishing the identified nodes, four groups were apparent. The four phenotypically similar groups of clusters aligned closely with canonical monocyte populations in peripheral blood, namely $CD14^{pos}CD16^{neg}$, $CD14^{pos}CD16^{pos}$, $CD14^{dim}CD16^{pos}Slan^{low}$, and $CD14^{dim}CD16^{pos}Slan^{high}$. These subsets comprised 85%, 9%, 3%, and 3% of monocytes respectively, as expected [12] (Figure 1C). Dendritic cell population SPADE nodes were recognized within the MPS gate as $HLA\text{-}DR^{high}CD123^{high}$ (pDC) or $HLA\text{-}DR^{high}CD11c^{high}$ (cDC), whereas polynuclear basophils (Pnb) were recognized as $HLA\text{-}DR^{low}CD123^{pos}$ (Figure S1B). Finally, the relative expression of additional markers across the monocyte subsets as obtained by mass cytometry was compared (Figure 1D). Both $Slan^{high}$ and $Slan^{low}$ subsets of non-classical monocytes expressed lower level of CD36, CD64, CCR2, and CD14, consistent with previously published data [12,48]. These observations confirmed that the panel design and analysis strategy captured well-established monocyte subtypes.

DCs-, MDSCs- and macrophages- derived *in vitro* from monocyte are profiled by CyTOF

Given that CD14 and CD16, the two central markers used to delineate monocyte subsets in the established nomenclature, show a continuous gradient of expression, we hypothesized that a high-dimensional approach would enhance the characterization of monocytic myeloid-derived suppressor cells (M-MDSC) and macrophage polarization subtypes. *In vitro* derived DCs, MDSCs, and macrophage subsets (M_b, M_LPS, M_IFNγ, M_IL4, M_IL10, M_IL6, and M_TPP) from peripheral blood monocytes were characterized as a comparison point for *in vivo* studies (Figure 2A). In vitro subsets were derived according to best practices for characterizing myeloid cell polarization [11,16,42]. After a SPADE analysis (Figure 2B), variation of cell abundance under stimulation in each node was summarized (Figure 2C). Before stimulation, monocytes comprised 98.6% of the MPS. Under appropriate stimulation, DC, MDSC, and M_b were increased from 0.1% to 76%, 87%, and 78%, respectively, in the MPS gate. After polarization, M_LPS, M_IFNg, M_IL4, M_IL10, M_IL6, and M_TPP were increased from less than 10% to 52%, 66%, 56%, 80%, 40%, and 81%, respectively. Interestingly, some conditions polarized monocytes to more than just one main population. For instance, M-CSF + LPS increased the percentage of cells in the both LPS gate from (0.9% to 53%) and TPP gate (from 3.2% to 22%) (Figure 2C). Finally, unclassified cells (i.e., those not included in any gate) were below 10% in all conditions. Of note, T cells were increased under IL-4, IFNγ, or IL-6 treatments (from 4% in the control to approximately 22% after culture).

MDSCs and polarized macrophages have specific phenotypes

Next, the phenotype of cells types obtained after differentiation of monocytes and polarization of macrophages was examined. To broadly assess the modulation of protein expression, median expression was assessed for each population (Figure 3A). Average transformed median expression was then calculated from nodes included in each gate identity (Figure 3B). Monocytes (Mo) were distinguished by high expression of CD33, CD36, and CCR2 and low CD163 and CD274 expression. DCs were $CD11c^{high}$ and $HLA\text{-}DR^{high}$. M_b were CD14, CD206, and HLA-DR positive. Statistical differences between all conditions are summarized in Figure S2. In particular, various polarized macrophages were compared to M_b (Figure 3C). M_LPS was distinguished by high levels of CD13 and CD86 and low level of CD163 and CD206 ($P < .01$). M_IL4 was $CD274^{high}$ and $CD64^{low}$ ($P<.01$). M_TPP expressed $CD14^{high}$ and $HL\text{-}DR^{low}$ ($P < .001$). M_IFNg was $CD64^{high}$ and $CD86^{high}$ ($P < .001$). M_IL10 was $CD14^{high}$, $CCR2^{high}$, and $CD163^{high}$ ($P < .01$), of note CD163 was significantly more expressed in M_IL10 than in M_b ($P < .01$) (Figure S2). Finally, M_IL6 was $CD11c^{high}$ and $CD33^{high}$ ($P < .05$). Then, MDSCs were compared to monocytes (Mo), DCs, and M_b (Figure 3C). MDSC showed higher expression of CD32, CD206, and CD13 ($P < .05$), and a lower expression of CD36, CD163, S100A9, CD33, and HLA-DR ($P < .05$), when compared to monocytes. Compared to DC, MDSC expressed higher amounts of CD32, CD206, CD64, CCR2, CD14 ($P < .05$) and lower amounts of CD13, CD274, CD33, and HLA-DR ($P < .05$). Finally, comparing MDSC to M_b, higher expression of CD64 and CCR2 was observed ($P < .05$) and lower expression of CD14, CD13, CD11c, CD36, CD163, S100A9, CD33, and HLA-DR was observed ($P < .05$). Peripheral blood derived MDSC were distinguished by the expected low expression of HLA-DR and by an unexpectedly

low expression of S100A9, in contrast to other peripheral blood mononuclear myeloid cell populations, with the exception of DCs.

MDSCs derived from bone marrow are S100A9^{pos}

Published protocols have established methods to derive MDSC, including combining cytokines or culturing peripheral blood or bone marrow. We derived MDSCs from bone marrow to investigate their phenotype following the protocol published by Marigo and colleagues [41]. As published, we cultured human bone marrow for 4 days with GM-CSF+G-CSF or GM-CSF+IL6 before CyTOF analysis (Figure 4A). Median protein expression is shown on hierarchically clustered heatmaps (Figure 4B). A first group of nodes (in green) was mainly CD11c^{pos}, CD11b^{pos}, CD36^{pos}, CD14^{pos} CD13^{pos}, CD64^{pos}, and HLA-DR^{pos} but also CD274^{pos} and CD86^{pos}. These cells displayed heterogeneous expression of S100A9, in particular node #7 (S100A9^{low}) was increased only with GM-CSF+G-CSF. One group of cells (in purple) displayed the expected MDSC phenotype (i.e. S100A9^{high} , CD33^{pos}, CD14^{pos} and HLA-DR^{low}), in addition, these cells were also CD64^{pos}, CD11b^{pos}, CCR2^{pos}, CD36^{pos}, CD13^{pos}, and CD32^{pos}. Of note, node #24 was only increased under GM-CSF and G-CSF and was characterized by a very high expression of CD32. Finally, a third group of nodes was found (in orange) in which cells were CD123^{pos} and HLA-DR^{pos}, while CD14, CD11b, CD36, CD64, and S100A9 were not expressed; thus, these cells were labeled DC (Figure 4B). The increase in abundance for these cells was assessed in 3 different human bone marrow samples. All three phenotypes (i.e. monocytes that were CD86^{pos} and CD274^{pos}, MDSC, and DC) were significantly increased after GM-CSF+G-CSF or GM-CSF+IL6 culture when compared to the vehicle (Figure 4C). No difference in cell frequency was found

between both conditions (Figure 4C). Finally, due to the phenotypic differences observed between MDSCs derived from PBMC and bone marrow, and to demonstrate their suppressive capabilities, an allogeneic three-way MLR assay was performed (Figure 5). MDSCs obtained were suppressive at ratio of 1:8, 1:4, and 1:2 when derived from bone marrows and 1:4 and 1:2 when derived from PBMCs ($p<.05$).

Mass cytometry identifies phenotypic MDSCs in the peripheral blood of melanoma patients

The mass cytometry panel, unsupervised analysis approach, and myeloid cell definitions were finally evaluated in clinical samples. MDSCs have previously been reported to be increased in peripheral blood from solid tumor patients irrespective of the disease stage, including melanoma patients [49-53]. Here, an abundance of cells with an MDSC phenotype including high S100A9 protein expression were observed in the peripheral blood of melanoma patients (Figure 6A). This cell type was significantly increased in 8 samples from 4 patients compared to HD, with abundance at 3% and 15.5% from the MPS gate, respectively ($P = .019$) (Figure 6B).

Discussion

The MPS compartment includes monocyte, DCs and macrophages, cells that are extremely heterogeneous in their phenotypes and functions. Recently, their nomenclature has been extensively revised and clarified [1,8,10,11]. As there are no unique identity markers and an overlap in their phenotype, their definition at the protein level still debated. Here, we hypothesized that mass cytometry data parsed by high dimensional approaches such as SPADE, viSNE, and hierarchical clustering, will clarify at the protein level the human spectrum of the MPS compartment. To this aim, various *in vitro* culture conditions and peripheral blood from cancer patients were compared to build a reference data framework including 1) monocyte subsets and MDSCs, 2) DCs, and 3) macrophages under basal conditions or treated with various canonical polarization stimuli.

To date, mass cytometry analyses have been performed on a limited number of myeloid populations. In human, peripheral blood, bone marrow, or tissues from HDs [21], inflammatory or septic patients [28,32,54,55], or patients suffering from acute myeloid leukemia (AML) [43,56-58] have been analyzed for myeloid cells. Noteworthy, except in AML, panels employed, were not dedicated specifically for in deep analysis of the myeloid compartment. Markers used in these studies included mostly CD13, CD33, CD36, CD14, CD16, HLA-DR, CD11b, CD11c, and CD123. In a recent comprehensive panel dedicated to the monitoring of immunomodulatory therapies on PBMCs, CD14, CD15, HLA-DR, CD11c, CD36, CD16, CD169, CD123, CD303, Siglec-8, and CD1c were proposed to delineate neutrophils, monocytes, basophils, eosinophils, as well as DC subsets [59]. In mice, more complete myeloid targeted panels have been published, in particular with the use of the specific myeloid markers F4/80, Ly6C, and Ly6G [29,60]. The panel was built by including 1)

canonical markers from prior studies of the human MPS [40], 2) markers know to be modulated in specific monocyte subsets or macrophages polarization stages (viz. CCR2, CD163, CD206, CD32, and CD64), and 3) markers differentially expressed during monocyte/DC activation (viz. CD86, CD274, CD45RA). The panel was validated on PBMC in recognizing in HDs, the 4 already described monocytes subsets ($CD14^{pos}CD16^{neg}$, $CD14^{pos}CD16^{pos}$, $CD14^{dim}CD16^{pos}Slan^{low}$, and $CD14^{dim}CD16^{pos}Slan^{high}$) [10,12].

Then, to explore the full spectrum of the MPS compartment, we took advantage of recent nomenclature papers [11], resource work refining the macrophage transcriptomic landscape [16], and studies on MDSCs [42] or on DCs [61,62]. In particular, Xue and colleagues described 9 different clusters of transcription networks [16]. We decided to align as much as possible with these conditions and thus derived from monocyte, M_b, M_IL4, M_IL10, M_LPS, M_IFNγ, M_IL6, and M_TPP, but also DCs and MDSCs given that their phenotypes are overlapping. Regarding macrophages, each stimulation condition gave rise to a specific phenotype of polarized macrophage (Figure 2B, C). There was no or little overlap between M_IFNg and M_LPS (both previously known as M1) and M_IL4 an M_IL10 (both previously known as M2). M_TPP also represented a separate cluster of nodes. This was in agreement with previous findings at the transcriptomic level, where macrophages polarized by IL4, IL10, IFNγ, and LPS clustered separately based on RNA expression profiles [16]. Novel patterns of phenotype within MPS were discovered and remarkable. CD32, CD14, CCR2, CD163, CD64, and CD33 were highly expressed in M_IL10. CD274 and CD86 were highly expressed, whereas CD14, CD32, and CD33 were expressed at low level in M_IL4 (Figure 2B, C and S2). Surprisingly, phenotype pattern of M_LPS and M_IL4 were separated only by CD32

and CD33, more expressed in M_LPS, whereas CD274 was less express, and CD163 was not differently expressed. CD163 is considered as a key marker of tumor-associated macrophages (TAM) and sometimes by extension for the historical M2 macrophages, however a higher expression in M_IL10 than in M_IL4 has been shown [63]. M_TPP expressed high levels of CD14 and CD13, whereas HLA-DR was expressed at low level and M_TPP were shown to be immuno-suppressive [16]. MDSCs were also clearly separated from M_b, DCs, and monocytes (Figure 2B-C) by especially high levels of CD32, CD206, CD64, CCR2, and CD14 and low levels of CD33 and HLA-DR. MDSCs were also phenotypically different form M_IL4, M_IL10, and M_TPP, three polarized macrophages with anti-inflammatory functions, due to higher expression of CCR2 and CD206 and lower expression of CD13 (Figure S2). Because HLA-DR expression is continuous across myeloid cells, M-MDSCs have been challenging to distinguish from monocytes in peripheral blood. Based on observations here, we propose using CD32, CD206, and S100A9 in addition to CD14 and HLA-DR (Figure 3C).

Surprisingly, S100A9, a highly expressed protein marker of MDSCs [8,64-66], was expressed at low levels in MDSCs generated from peripheral blood (Figure 3B, C). Despite lower S100A9 than other MDSCs, peripheral blood derived MDSCs were functional and effective at suppressing T cell proliferation (Figure 5). In previous works, human MDSCs were derived either from peripheral blood or from bone marrow [41,42]. Thus we hypothesized that MDSC derived from bone marrow would have a different phenotype. Monocytes, DCs, and MDSCs were increased in abundance when bone marrow were cultured with GM-CSF + G-CSF or with GM-CSF + IL6 (Figure 4C). This observation has not been reported in published protocols to derive MDSCs and would have been difficult to identify without the single cell high-

dimensional mass cytometry approach. In agreement, it has been shown recently that GM-CSF cultured murine bone marrow generated both macrophage and DC [62]. We also found that MDSCs derived from human marrow expressed a more consistent phenotype, highly expressing S100A9, CD14, CD64, CD11b, CCR2, CD32 while remaining HLA-DR^{low}, making BM MDSCs an ideal, if less practical to obtain, reference point. Finally, this approach was employed to characterize clinical samples from melanoma patients because in this cancer high level of circulating MDSC have been described across grades [49,53]. MDSCs with the same phenotype as those derived from bone marrow were enriched in the blood of melanoma patients.

In summary, a broad phenotypic analysis of the human MPS compartment characterizes know cell populations and brings increased clarity to the definitions of cell types including MDSC and polarized mononuclear phagocytes. In particular, the multidimensional approach at the protein level might constitute the first step of efforts in unifying transcriptomic to proteomic and functional approaches in a multi-OMICs era [67]. It would be interesting to expand the panel in order to have a clear view of signaling pathways involved. Finally, this study also highlights the potential value of mass cytometry in system immune monitoring of the myeloid compartment for patients in clinical trials.

Author contribution

M.R. and J.M.I. conceived the study. M.R., P.B.F., A.R.G., F.L., and S.L.G., performed experiments. D.B.J. provided samples. M.R., P.B.F., A.R.G., F.L., S.L.G., K.E.D., and J.M.I. analyzed data and revised figures. M.R. and J.M.I. wrote the paper and all authors revised the manuscript.

Acknowledgment

MR is the recipient of a fellowship from the Nuovo-Soldati Foundation (Switzerland). This study was supported by F31 CA199993 (A.R.G.), K12 CA090625 (P.B.F.), R25 CA136440-04 (K.E.D.), R00 CA143231-03 (J.M.I.), the Vanderbilt-Ingram Cancer Center (VICC, P30 CA68485), VICC Ambassadors, a VICC Hematology Helping Hands award (J.M.I., P.B.F., and K.E.D.), and the Tinsley R. Harrison Society (P.B.F.). The authors thank Emmanuel Gautherot from Beckman Coulter Immunotech (Marseille France) for the gift of purified CD206.

Conflict of Interest Disclosure

J.M.I. is co-founder and board member and Cytobank Inc. and received research support from Incyte Corp and Janssen.

References

[1] Guilliams, M., Ginhoux, F., Jakubzick, C., Naik, S.H., Onai, N., Schraml, B.U., Segura, E., Tussiwand, R., Yona, S. (2014) Dendritic cells, monocytes and macrophages: a unified nomenclature based on ontogeny. *Nature Reviews Immunology*. 14,571–578.

[2] Engblom, C., Pfirschke, C., Pittet, M.J. (2016) The role of myeloid cells in cancer therapies. *Nature Reviews Cancer*. 16,447–462.

[3] Lavin, Y., Mortha, A., Rahman, A., Merad, M. (2015) Regulation of macrophage development and function in peripheral tissues. *Nature Reviews Immunology*. 15,731–744.

[4] Merad, M., Sathe, P., Helft, J., Miller, J., Mortha, A. (2013) The dendritic cell lineage: ontogeny and function of dendritic cells and their subsets in the steady state and the inflamed setting. *Annual Review of Immunology*. 31,563–604.

[5] Taylor, P.R., Martinez-Pomares, L., Stacey, M., Lin, H.-H., Brown, G.D., Gordon, S. (2005) Macrophage receptors and immune recognition. *Annual Review of Immunology*. 23,901–944.

[6] Hamann, J., Koning, N., Pouwels, W., Ulfman, L.H., van Eijk, M., Stacey, M., Lin, H.-H., Gordon, S., Kwakkenbos, M.J. (2007) EMR1, the human homolog of F4/80, is an eosinophil-specific receptor. *European Journal of Immunology*. 37,2797–2802.

[7] Rabinovich, G.A., Gabrilovich, D.I., Sotomayor, E.M. (2007) Immunosuppressive strategies that are mediated by tumor cells. *Annual Review of Immunology*. 25,267–296.

[8] Bronte, V., Brandau, S., Chen, S.-H., Colombo, M.P., Frey, A.B., Greten,

T.F., Mandruzzato, S., Murray, P.J., Ochoa, A., Ostrand-Rosenberg, S., Rodriguez, P.C., Sica, A., Umansky, V., Vonderheide, R.H., Gabrilovich, D.I. (2016) Recommendations for myeloid-derived suppressor cell nomenclature and characterization standards. *Nature Communications*. 7,12150.

[9] Ancuta, P. (2015) A slan-based nomenclature for monocytes? *Blood*. 126,2536–2538.

[10] Ziegler-Heitbrock, L., Ancuta, P., Crowe, S., Dalod, M., Grau, V., Hart, D.N., Leenen, P.J.M., Liu, Y.-J., MacPherson, G., Randolph, G.J., Scherberich, J., Schmitz, J., Shortman, K., Sozzani, S., Strobl, H., Zembala, M., Austyn, J.M., Lutz, M.B. (2010) Nomenclature of monocytes and dendritic cells in blood. *Blood*. 116,e74–80.

[11] Murray, P.J., Allen, J.E., Biswas, S.K., Fisher, E.A., Gilroy, D.W., Goerdt, S., Gordon, S., Hamilton, J.A., Ivashkiv, L.B., Lawrence, T., Locati, M., Mantovani, A., Martinez, F.O., Mege, J.-L., Mosser, D.M., Natoli, G., Saeij, J.P., Schultze, J.L., Shirey, K.A., Sica, A., Suttles, J., Udalova, I., Van Ginderachter, J.A., Vogel, S.N., Wynn, T.A. (2014) Macrophage activation and polarization: nomenclature and experimental guidelines. *Immunity*. 41,14–20.

[12] Cros, J., Cagnard, N., Woollard, K., Patey, N., Zhang, S.-Y., Senechal, B., Puel, A., Biswas, S.K., Moshous, D., Picard, C., Jais, J.-P., D'cruz, D., Casanova, J.-L., Trouillet, C., Geissmann, F. (2010) Human CD14dim Monocytes Patrol and Sense Nucleic Acids and Viruses via TLR7 and TLR8 Receptors. *Immunity*. 33,375–386.

[13] De Palma, M., Venneri, M.A., Galli, R., Sergi Sergi, L., Politi, L.S., Sampaolesi, M., Naldini, L. (2005) Tie2 identifies a hematopoietic lineage of

proangiogenic monocytes required for tumor vessel formation and a mesenchymal population of pericyte progenitors. *Cancer Cell*. 8,211–226.

[14] Martinez, F.O., Gordon, S., Locati, M., Mantovani, A. (2006) Transcriptional profiling of the human monocyte-to-macrophage differentiation and polarization: new molecules and patterns of gene expression. *Journal of Immunology*. 177,7303–7311.

[15] Ginhoux, F., Schultze, J.L., Murray, P.J., Ochando, J., Biswas, S.K. (2015) New insights into the multidimensional concept of macrophage ontogeny, activation and function. *Nature Immunology*. 17,34–40.

[16] Xue, J., Schmidt, S.V., Sander, J., Draffehn, A., Krebs, W., Quester, I., De Nardo, D., Gohel, T.D., Emde, M., Schmidleithner, L., Ganesan, H., Nino-Castro, A., Mallmann, M.R., Labzin, L., Theis, H., Kraut, M., Beyer, M., Latz, E., Freeman, T.C., Ulas, T., Schultze, J.L. (2014) Transcriptome-based network analysis reveals a spectrum model of human macrophage activation. *Immunity*. 40,274–288.

[17] Mosser, D.M., Edwards, J.P. (2008) Exploring the full spectrum of macrophage activation. *Nature Reviews Immunology*. 8,958–969.

[18] Edwards, J.P., Zhang, X., Frauwirth, K.A., Mosser, D.M. (2006) Biochemical and functional characterization of three activated macrophage populations. *Journal of Leukocyte Biology*. 80,1298–1307.

[19] Biswas, S.K., Allavena, P., Mantovani, A. (2013) Tumor-associated macrophages: functional diversity, clinical significance, and open questions. *Seminars in Immunopathology*. 35,585–600.

[20] Greenplate, A.R., Johnson, D.B., Roussel, M., Savona, M.R., Sosman, J.A., Puzanov, I., Ferrell, P.B., Irish, J.M. (2016) Myelodysplastic Syndrome

Revealed by Systems Immunology in a Melanoma Patient Undergoing Anti-PD-1 Therapy. *Cancer Immunology Research*. 4,474–480.

[21] Bendall, S.C., Simonds, E.F., Qiu, P., Amir, E.A.D., Krutzik, P.O., Finck, R., Bruggner, R.V., Melamed, R., Trejo, A., Ornatsky, O.I., Balderas, R.S., Plevritis, S.K., Sachs, K., Pe'er, D., Tanner, S.D., Nolan, G.P. (2011) Single-Cell Mass Cytometry of Differential Immune and Drug Responses Across a Human Hematopoietic Continuum. *Science*. 332,687–696.

[22] Spitzer, M.H., Nolan, G.P. (2016) Mass Cytometry: Single Cells, Many Features. *Cell*. 165,780–791.

[23] Saeys, Y., Gassen, S.V., Lambrecht, B.N. (2016) Computational flow cytometry: helping to make sense of high-dimensional immunology data. *Nature Reviews Immunology*. 16,449–462.

[24] Diggins, K.E., Greenplate, A.R., Leelatian, N., Wogsland, C.E., Irish, J.M. (2017) Characterizing cell subsets using marker enrichment modeling. *Nature Methods*. 14,275–278.

[25] Amir, E.-A.D., Davis, K.L., Tadmor, M.D., Simonds, E.F., Levine, J.H., Bendall, S.C., Shenfeld, D.K., Krishnaswamy, S., Nolan, G.P., Pe'er, D. (2013) viSNE enables visualization of high dimensional single-cell data and reveals phenotypic heterogeneity of leukemia. *Nature Biotechnology*. 31,545–552.

[26] Qiu, P., Simonds, E.F., Bendall, S.C., Gibbs, K.D., Bruggner, R.V., Linderman, M.D., Sachs, K., Nolan, G.P., Plevritis, S.K. (2011) Extracting a cellular hierarchy from high-dimensional cytometry data with SPADE. *Nature Biotechnology*. 29,886–891.

[27] Wong, M.T., Chen, J., Narayanan, S., Lin, W., Anicete, R., Kiaang, H.T.K., De

Lafaille, M.A.C., Poidinger, M., Newell, E.W. (2015) Mapping the Diversity of Follicular Helper T Cells in Human Blood and Tonsils Using High-Dimensional Mass Cytometry Analysis. *Cell Reports*. 11,1822–1833.

[28] van Unen, V., Li, N., Molendijk, I., Temurhan, M., Höllt, T., van der Meulen-de Jong, A.E., Verspaget, H.W., Mearin, M.L., Mulder, C.J., van Bergen, J., Lelieveldt, B.P.F., Koning, F. (2016) Mass Cytometry of the Human Mucosal Immune System Identifies Tissue- and Disease-Associated Immune Subsets. *Immunity*. 44,1227–1239.

[29] Becher, B., Schlitzer, A., Chen, J., Mair, F., Sumatoh, H.R., Teng, K.W.W., Low, D., Ruedl, C., Riccardi-Castagnoli, P., Poidinger, M., Greter, M., Ginhoux, F., Newell, E.W. (2014) High-dimensional analysis of the murine myeloid cell system. *Nature Immunology*. 15,1181–1189.

[30] Sen, N., Mukherjee, G., Sen, A., Bendall, S.C., Sung, P., Nolan, G.P., Arvin, A.M. (2014) Single-Cell Mass Cytometry Analysis of Human Tonsil T Cell Remodeling by Varicella Zoster Virus. *Cell Reports*. 8,633–645.

[31] Horowitz, A., Strauss-Albee, D.M., Leipold, M., Kubo, J., Nemat-Gorgani, N., Dogan, O.C., Dekker, C.L., Mackey, S., Maecker, H., Swan, G.E., Davis, M.M., Norman, P.J., Guethlein, L.A., Desai, M., Parham, P., Blish, C.A. (2013) Genetic and environmental determinants of human NK cell diversity revealed by mass cytometry. *Science Translational Medicine*. 5,208ra145.

[32] Gaudilliere, B., Fragiadakis, G.K., Bruggner, R.V., Nicolau, M., Finck, R., Tingle, M., Silva, J., Ganio, E.A., Yeh, C.G., Maloney, W.J., Huddleston, J.I., Goodman, S.B., Davis, M.M., Bendall, S.C., Fantl, W.J., Angst, M.S., Nolan, G.P. (2014) Clinical recovery from surgery correlates with single-cell immune signatures. *Science Translational Medicine*. 6,255ra131–255ra131.

[33] Mason, G.M., Lowe, K., Melchiotti, R., Ellis, R., de Rinaldis, E., Peakman, M., Heck, S., Lombardi, G., Tree, T.I.M. (2015) Phenotypic Complexity of the Human Regulatory T Cell Compartment Revealed by Mass Cytometry. *The Journal of Immunology*. 195,2030–2037.

[34] Hansmann, L., Blum, L., Ju, C.-H., Liedtke, M., Robinson, W.H., Davis, M.M. (2015) Mass cytometry analysis shows that a novel memory phenotype B cell is expanded in multiple myeloma. *Cancer Immunology Research*. 3,650–660.

[35] Strauss-Albee, D.M., Horowitz, A., Parham, P., Blish, C.A. (2014) Coordinated regulation of NK receptor expression in the maturing human immune system. *The Journal of Immunology*. 193,4871–4879.

[36] Bendall, S.C., Davis, K.L., Amir, E.-A.D., Tadmor, M.D., Simonds, E.F., Chen, T.J., Shenfeld, D.K., Nolan, G.P., Pe'er, D. (2014) Single-Cell Trajectory DetectionUncovers Progression and Regulatory Coordination in Human B Cell Development. *Cell*. 157,714–725.

[37] Nicholas, K.J., Greenplate, A.R., Flaherty, D.K., Matlock, B.K., Juan, J.S., Smith, R.M., Irish, J.M., Kalams, S.A. (2016) Multiparameter analysis of stimulated human peripheral blood mononuclear cells: A comparison of mass and fluorescence cytometry. *Cytometry Part a : the Journal of the International Society for Analytical Cytology*. 89,271–280.

[38] Guilliams, M., Dutertre, C.-A., Scott, C.L., McGovern, N., Sichien, D., Chakarov, S., Van Gassen, S., Chen, J., Poidinger, M., De Prijck, S., Tavernier, S.J., Low, I., Irac, S.E., Mattar, C.N., Sumatoh, H.R., Low, G.H.L., Chung, T.J.K., Chan, D.K.H., Tan, K.K., Hon, T.L.K., Fossum, E., Bogen, B., Choolani, M., Chan, J.K.Y., Larbi, A., Luche, H., Henri, S., Saeys, Y., Newell, E.W., Lambrecht, B.N., Malissen, B., Ginhoux, F. (2016) Unsupervised High-

Dimensional Analysis Aligns Dendritic Cells across Tissues and Species. *Immunity*. 45,669–684.

[39] Irish, J.M. (2014) Beyond the age of cellular discovery. *Nature Immunology*. 15,1095–1097.

[40] Roussel, M., Greenplate, A.R., Irish, J.M. (2016) Dissecting Complex Cellular Systems with High Dimensional Single Cell Mass Cytometry.

[41] Marigo, I., Bosio, E., Solito, S., Mesa, C., Fernández, A., Dolcetti, L., Ugel, S., Sonda, N., Bicciato, S., Falisi, E., Calabrese, F., Basso, G., Zanovello, P., Cozzi, E., Mandruzzato, S., Bronte, V. (2010) Tumor-induced tolerance and immune suppression depend on the C/EBPbeta transcription factor. *Immunity*. 32,790–802.

[42] Lechner, M.G., Liebertz, D.J., Epstein, A.L. (2010) Characterization of Cytokine-Induced Myeloid-Derived Suppressor Cells from Normal Human Peripheral Blood Mononuclear Cells. *The Journal of Immunology*. 185,2273–2284.

[43] Ferrell, P.B., Diggins, K.E., Polikowsky, H.G., Mohan, S.R., Seegmiller, A.C., Irish, J.M. (2016) High-Dimensional Analysis of Acute Myeloid Leukemia Reveals Phenotypic Changes in Persistent Cells during Induction Therapy. *PLoS ONE*. 11,e0153207.

[44] Fienberg, H.G., Simonds, E.F., Fantl, W.J., Nolan, G.P., Bodenmiller, B. (2012) A platinum-based covalent viability reagent for single-cell mass cytometry. *Cytometry Part a : the Journal of the International Society for Analytical Cytology*. 81,467–475.

[45] Finck, R., Simonds, E.F., Jager, A., Krishnaswamy, S., Sachs, K., Fantl, W., Pe'er, D., Nolan, G.P., Bendall, S.C. (2013) Normalization of mass cytometry

data with bead standards. *Cytometry Part a : the Journal of the International Society for Analytical Cytology*. 83,483–494.

[46] Diggins, K.E., Ferrell, P.B., Irish, J.M. (2015) Methods for discovery and characterization of cell subsets in high dimensional mass cytometry data. *Methods*. 82,55–63.

[47] Kotecha, N., Krutzik, P.O., Irish, J.M. (2010) Web-based analysis and publication of flow cytometry experiments. *Current Protocols in Cytometry / Editorial Board, J Paul Robinson, Managing Editor*. Chapter 10,100708 Unit10.17–10.17.24.

[48] Hofer, T.P., Zawada, A.M., Frankenberger, M., Skokann, K., Satzl, A.A., Gesierich, W., Schuberth, M., Levin, J., Danek, A., Rotter, B., Heine, G.H., Ziegler-Heitbrock, L. (2015) slan-defined subsets of CD16-positive monocytes: impact of granulomatous inflammation and M-CSF receptor mutation. *Blood*. 126,2601–2610.

[49] Sade-Feldman, M., Kanterman, J., Klieger, Y., Ish-Shalom, E., Olga, M., Saragovi, A., Shtainberg, H., Lotem, M., Baniyash, M. (2016) Clinical Significance of Circulating CD33+CD11b+HLA-DR- Myeloid Cells in Patients with Stage IV Melanoma Treated with Ipilimumab. *Clinical Cancer Research*. 22,5661–5672.

[50] Rudolph, B.M., Loquai, C., Gerwe, A., Bacher, N., Steinbrink, K., Grabbe, S., Tuettenberg, A. (2014) Increased frequencies of CD11b +CD33 +CD14 +HLA-DR lowmyeloid-derived suppressor cells are an early event in melanoma patients. *Experimental Dermatology*. 23,202–204.

[51] Chevolet, I., Speeckaert, R., Schreuer, M., Neyns, B., Krysko, O., Bachert, C., Van Gele, M., van Geel, N., Brochez, L. (2015) Clinical significance of

plasmacytoid dendritic cells and myeloid-derived suppressor cells in melanoma. *Journal of Translational Medicine*. 13,9.

[52] Weide, B., Martens, A., Zelba, H., Stutz, C., Derhovanessian, E., Di Giacomo, A.M., Maio, M., Sucker, A., Schilling, B., Schadendorf, D., Büttner, P., Garbe, C., Pawelec, G. (2014) Myeloid-derived suppressor cells predict survival of patients with advanced melanoma: comparison with regulatory T cells and NY-ESO-1- or melan-A-specific T cells. *Clinical Cancer Research*. 20,1601–1609.

[53] Mao, Y., Poschke, I., Wennerberg, E., Pico de Coana, Y., Egyhazi Brage, S., Schultz, I., Hansson, J., Masucci, G., Lundqvist, A., Kiessling, R. (2013) Melanoma-Educated CD14+ Cells Acquire a Myeloid-Derived Suppressor Cell Phenotype through COX-2-Dependent Mechanisms. *Cancer Research*. 73,3877–3887.

[54] Mingueneau, M., Boudaoud, S., Haskett, S., Reynolds, T.L., Nocturne, G., Norton, E., Zhang, X., Constant, M., Park, D., Wang, W., Lazure, T., Le Pajolec, C., Ergun, A., Mariette, X. (2016) Cytometry by time-of-flight immunophenotyping identifies a blood Sjögren's signature correlating with disease activity and glandular inflammation. *The Journal of Allergy and Clinical Immunology*. 137,1809–1821.e12.

[55] Gaudilliere, B., Ganio, E.A., Tingle, M., Lancero, H.L., Fragiadakis, G.K., Baca, Q.J., Aghaeepour, N., Wong, R.J., Quaintance, C., El-Sayed, Y.Y., Shaw, G.M., Lewis, D.B., Stevenson, D.K., Nolan, G.P., Angst, M.S. (2015) Implementing Mass Cytometry at the Bedside to Study the Immunological Basis of Human Diseases: Distinctive Immune Features in Patients with a History of Term or Preterm Birth. *Cytometry Part a : the Journal of the*

International Society for Analytical Cytology. 87,817–829.

[56] Behbehani, G.K., Samusik, N., Bjornson, Z.B., Fantl, W.J., Medeiros, B.C., Nolan, G.P. (2015) Mass Cytometric Functional Profiling of Acute Myeloid Leukemia Defines Cell-Cycle and Immunophenotypic Properties That Correlate with Known Responses to Therapy. *Cancer Discovery*. 5,988–1003.

[57] Levine, J.H., Simonds, E.F., Bendall, S.C., Davis, K.L., Amir, E.-A.D., Tadmor, M.D., Litvin, O., Fienberg, H.G., Jager, A., Zunder, E.R., Finck, R., Gedman, A.L., Radtke, I., Downing, J.R., Pe'er, D., Nolan, G.P. (2015) Data-Driven Phenotypic Dissection of AML Reveals Progenitor-like Cells that Correlate with Prognosis. *Cell*. 162,184–197.

[58] Han, L., Qiu, P., Zeng, Z., Jorgensen, J.L., Mak, D.H., Burks, J.K., Schober, W., McQueen, T.J., Cortes, J., Tanner, S.D., Roboz, G.J., Kantarjian, H.M., Kornblau, S.M., Guzman, M.L., Andreeff, M., Konopleva, M. (2015) Single-cell mass cytometry reveals intracellular survival/proliferative signaling in FLT3-ITD-mutated AML stem/progenitor cells. *Cytometry Part a : the Journal of the International Society for Analytical Cytology*. 87,346–356.

[59] Baumgart, S., Peddinghaus, A., Schulte-Wrede, U., Mei, H.E., Grützkau, A. (2016) OMIP-034: Comprehensive immune phenotyping of human peripheral leukocytes by mass cytometry for monitoring immunomodulatory therapies. *Cytometry Part a : the Journal of the International Society for Analytical Cytology*.51–5.

[60] Spitzer, M.H., Gherardini, P.F., Fragiadakis, G.K., Bhattacharya, N., Yuan, R.T., Hotson, A.N., Finck, R., Carmi, Y., Zunder, E.R., Fantl, W.J., Bendall, S.C., Engleman, E.G., Nolan, G.P. (2015) IMMUNOLOGY. An interactive reference framework for modeling a dynamic immune system. *Science*.

349,1259425–1259425.

[61] Son, Y.-I., Egawa, S.-I., Tatsumi, T., Redlinger, R.E., Kalinski, P., Kanto, T. (2002) A novel bulk-culture method for generating mature dendritic cells from mouse bone marrow cells. *Journal of Immunological Methods*. 262,145–157.

[62] Helft, J., Böttcher, J., Chakravarty, P., Zelenay, S., Huotari, J., Schraml, B.U., Goubau, D., Sousa, C.R.E. (2015) GM-CSF Mouse Bone Marrow Cultures Comprise a Heterogeneous Population of CD11c. *Immunity*. 42,1197–1211.

[63] van de Garde, M.D.B., Martinez, F.O., Melgert, B.N., Hylkema, M.N., Jonkers, R.E., Hamann, J. (2014) Chronic Exposure to Glucocorticoids Shapes Gene Expression and Modulates Innate and Adaptive Activation Pathways in Macrophages with Distinct Changes in Leukocyte Attraction. *Journal of Immunology*. 192,1196–1208.

[64] Feng, P.-H., Lee, K.-Y., Chang, Y.-L., Chan, Y.-F., Kuo, L.-W., Lin, T.-Y., Chung, F.-T., Kuo, C.-S., Yu, C.-T., Lin, S.-M., Wang, C.-H., Chou, C.-L., Huang, C.-D., Kuo, H.-P. (2012) CD14(+)S100A9(+) monocytic myeloid-derived suppressor cells and their clinical relevance in non-small cell lung cancer. *American Journal of Respiratory and Critical Care Medicine*. 186,1025–1036.

[65] Zhao, F., Hoechst, B., Duffy, A., Gamrekelashvili, J., Fioravanti, S., Manns, M.P., Greten, T.F., Korangy, F. (2012) S100A9 a new marker for monocytic human myeloid-derived suppressor cells. *Immunology*. 136,176–183.

[66] Chen, X., Eksioglu, E.A., Zhou, J., Zhang, L., Djeu, J., Fortenbery, N., Epling-Burnette, P., Van Bijnen, S., Dolstra, H., Cannon, J., Youn, J.-I., Donatelli, S.S., Qin, D., De Witte, T., Tao, J., Wang, H., Cheng, P., Gabrilovich, D.I., List, A., Wei, S. (2013) Induction of myelodysplasia by myeloid-derived

suppressor cells. *The Journal of Clinical Investigation*. 123,4595–4611.

[67] Gordon, S., Plüddemann, A., Martinez Estrada, F. (2014) Macrophage heterogeneity in tissues: phenotypic diversity and functions. *Immunological Reviews*. 262,36–55.

Figure

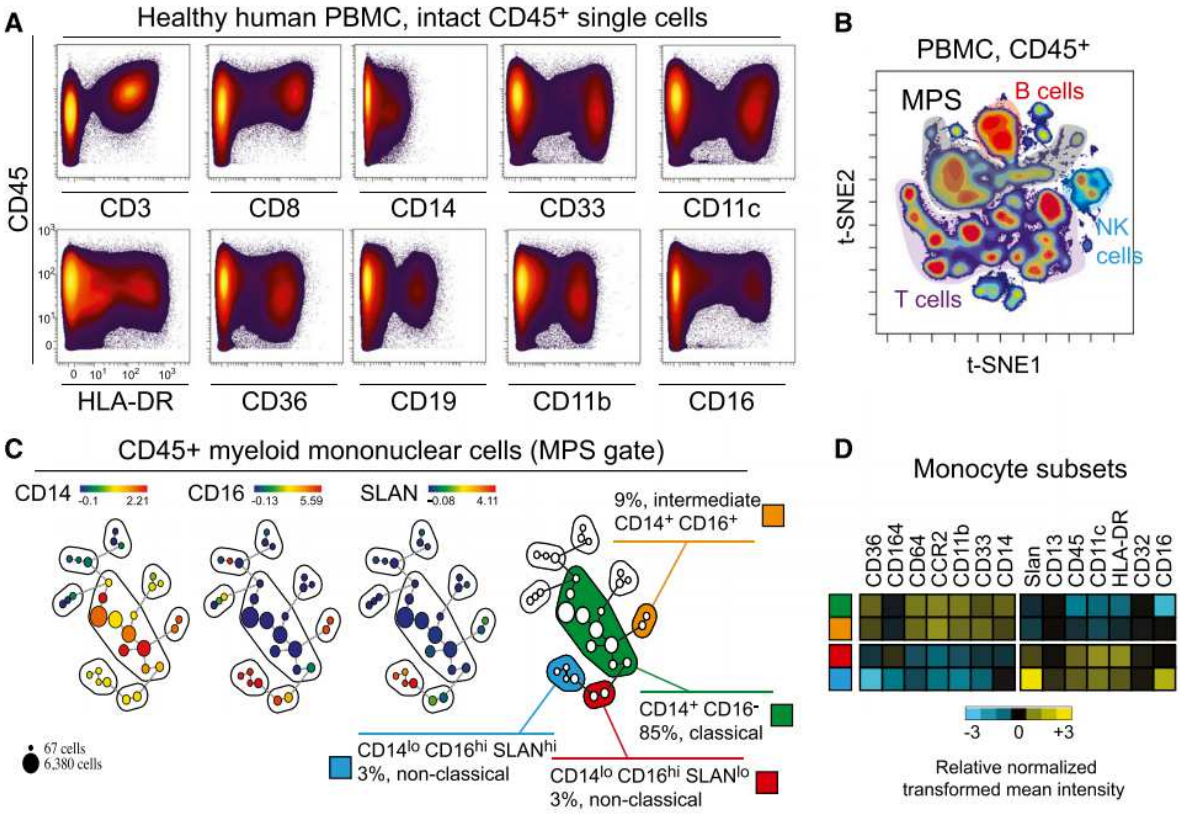

Figure 1: CyTOF panel and workflow analysis delineates four monocyte subsets in peripheral blood. (**A**) Biaxial plots showing the expression of markers on $Ir^{pos}CD45^{pos}$ PBMC measured by mass cytometry. A representative healthy donor is shown. An arcsinh scale (-5.0 to 10^4) with a cofactor of 5 was used. (**B**) By mass cytometry analysis >100,000 $Ir^{pos}CD45^{pos}$ cells were defined on a biaxial plot, before classification on a viSNE algorithm. MPS (>20,000 cells) was gated as remaining cells after the exclusion of B- ($CD19^{pos}$), T- ($CD3^{pos}$), and NK- ($CD3^{neg}CD16^{pos}CD45RA^{pos}$) lymphocytes and doublets (see Figure S1). (**C**) Events in the MPS gate were then parsed with SPADE into 30 nodes using all clustering markers except CD19 and CD3. $CD14^{pos}$-, $CD16^{pos}$-, and $Slan^{pos}$- SPADE groups were observed to match classical- ($CD14^{pos}CD16^{neg}$), intermediate- ($CD14^{pos}CD16^{pos}$), non-classical $Slan^{low}$- ($CD14^{dim}CD16^{pos}Slan^{low}$), and non-classical $Slan^{pos}$- ($CD14^{dim}CD16^{pos}Slan^{high}$) monocytes. A representative healthy donor is shown. % represents the frequency among PBMC. (**D**) On the 4 monocyte subsets

previously described in (B), heat maps showing the relative normalized transformed mean intensity for various markers tested by mass cytometry, for a representative healthy donor.

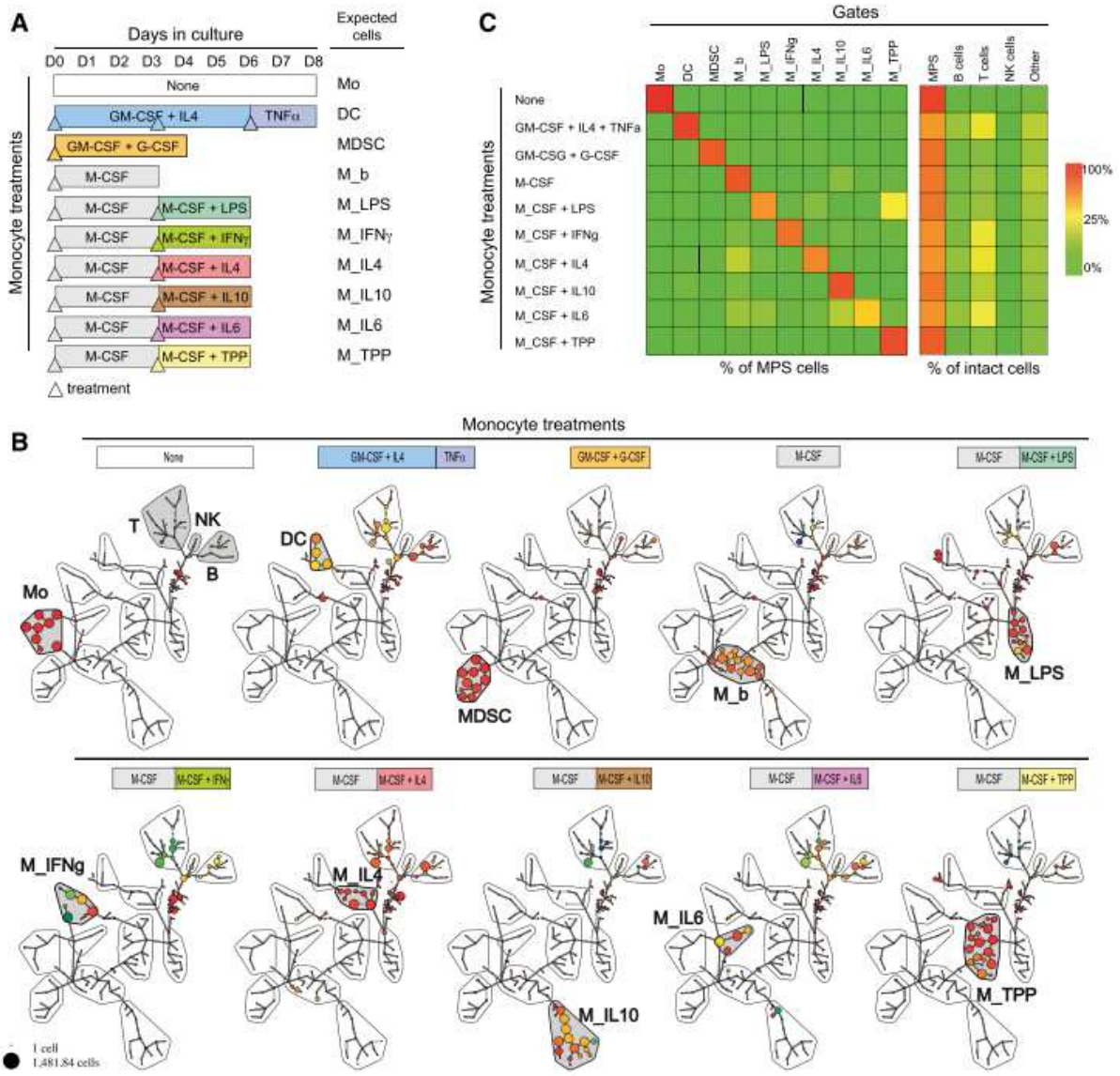

Figure 2: CyTOF profiles DCs-, MDSCs- and macrophages- derived *in vitro* from monocyte

(**A**) Experimental procedure to derived DC, MDSC, and macrophage at baseline (M_b) or polarized under various stimuli (M_LPS, M_IFNγ, M_IL4, M_IL10, M_IL6, and M_TPP [a cocktail including TNFα, PGE2, and Pam3]). Peripheral blood monocytes were obtained from blood donors and purified by elutriation. Expected cells from the stimuli condition are indicated on the right. Days of treatment (colored up-pointing triangle) or of collection (black down-pointing triangle) were specific to the

culture condition. (**B**) After CyTOF analysis, cells were defined as $Ir^{pos}CD45^{pos}$. Then, a SPADE analysis with 200 nodes and downsampling at 10% was performed. Adjacent nodes with an increase in cells abundance and phenotypic similarity were labeled in red with the name of expected cells from the culture condition. Mo, DC, MDSC, M_b, M_LPS, M_IFNγ, M_IL4, M_IL10, M_IL6, and M_TPP gates are positive for myeloid markers whereas T-, NK-, and B- gates expressed CD3, CD16/CD45RA, CD19, respectively. Nodes outside gates were considered as unclassified (**C**) *Left*- Cell abundance in gate (Mo, DC, MDSC, M_b, M_LPS, M_IFNγ, M_IL4, M_IL10, M_IL6, and M_TPP) reported to MPS gate and related to each condition of stimulation. *Right*- Cell abundance in Mo, DC, MDSC, M_b, M_LPS, M_IFNγ, M_IL4, M_IL10, M_IL6, and M_TPP gates (sum in MPS) and B-, T-, NK gate or unclassified, reported to intact cells ($Ir^{pos}CD45^{pos}$) and related to each condition of stimulation. Average percentage of 2 independent experiments.

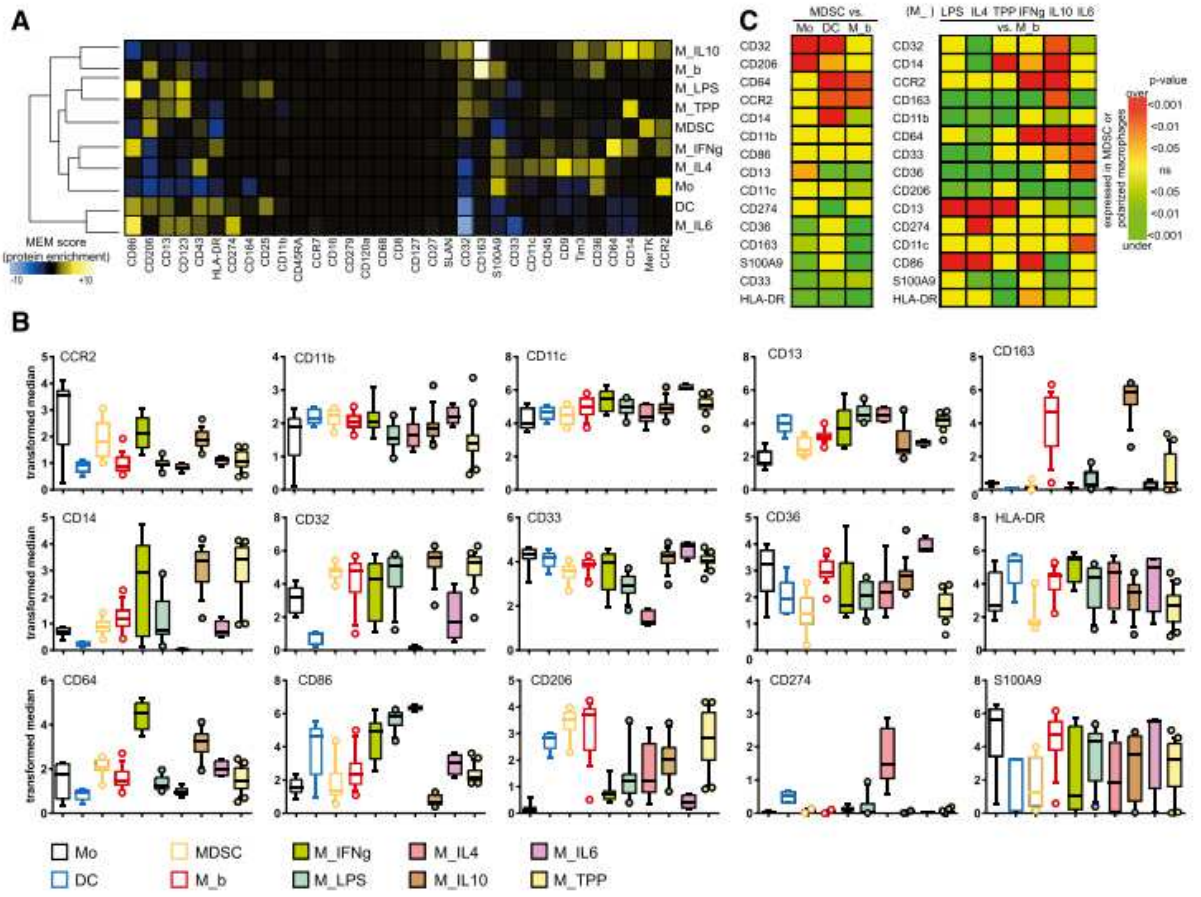

Figure 3: MDSC and polarized macrophages derived *in vitro* have specific phenotypes

(**A**) For Mo, DC, MDSC, M_b, M_LPS, M_IFNγ, M_IL4, M_IL10, M_IL6, and M_TPP gates, transformed median expression for each marker was averaged from all nodes included in the gate. After normalization, results are shown on heat map after hierarchical clustering. (**B**) Comparison of markers for each node (each dot represents a node). Box and Whisker plots with the 10-90 percentiles and the outliers are shown. Nodes from 2 or 3 different experiments are shown. One-way ANOVA tests (parametric or nonparametric as appropriate after normality test) with post test comparing all pairs of columns are summarized in Figure S2. (**C**) *Left*- Comparison of p-values between MDSC and monocyte (Mo), dendritic cells (DC), and M_b and *Right*- comparison of various polarized macrophage (M_IFNg, M_LPS, M_IL4, M_IL10, M_IL6, M_TPP) to M_b. Rows and columns were arranged after hierarchical clustering (not shown). Only markers at least once statistically different are shown. Unpaired t-tests (parametric or nonparametric as appropriate after normality test) were performed. Yellow: non-significant (ns); Light to dark green: significantly underexpressed in MDSC or polarized macrophages; Orange to red: significantly overexpressed in MDSC or polarized macrophages.

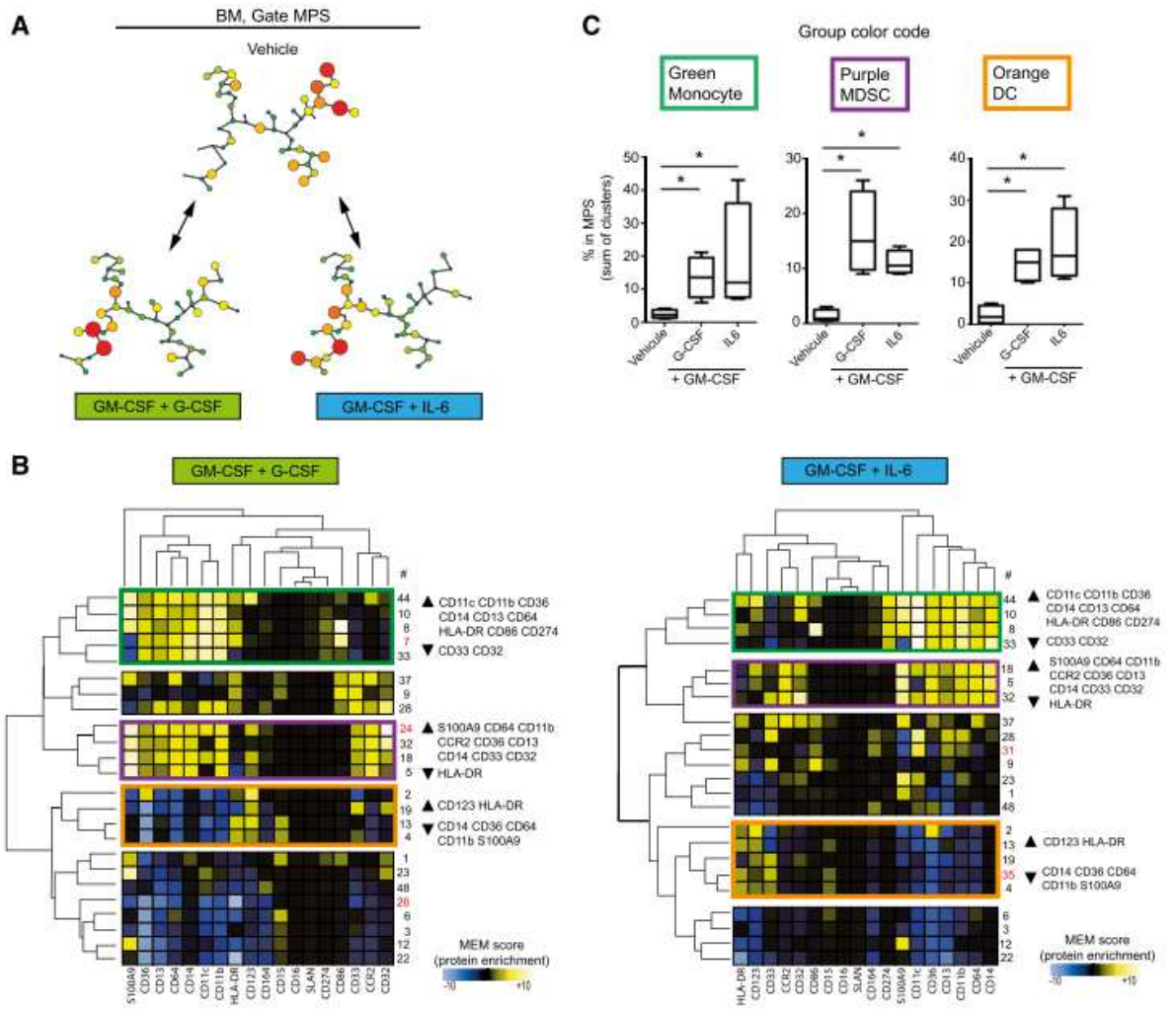

Figure 4: MDSCs obtained from bone marrow are S100A9^{pos}

(**A**) Human bone marrow was cultured for 4 days with GM-CSF+IL6 or GM-CSF+G-CSF or with the vehicle. By mass cytometry analysis >100,000 Ir^{pos}CD45^{pos} cells were defined on a biaxial plot, before classification on a viSNE algorithm. MPS (>20,000 cells) was gated as remaining cells after the exclusion of B- (CD19^{pos}), T- (CD3^{pos}), and NK- (CD3^{neg}CD16^{pos}CD45RA^{pos}) lymphocytes and doublets. Events in the MPS gate were then parsed with SPADE arbitrary restricted to 50 nodes using all clustering markers but CD19 and CD3. Then comparisons were made between each culture conditions and cells treated with vehicle. Nodes with a 2 fold increase in cell abundance (percentage FC>1) between GM-CSF+G-CSF and vehicle or between GM-CSF+IL6 were retained for further analysis (**B**) Transformed median expression for each markers was averaged from each nodes (percentage FC>1). After normalization, results are shown on heat map after hierarchical clustering. *Left-*

Nodes with an increase in cell abundance after GM-CSF+G-CSF culture. *Right-* Nodes with an increase in cell abundance after GM-CSF+IL6 culture. # nodes ID; in red: nodes increased in only one condition. Rectangles in green, purple, or orange indicate various phenotype of interest. A representative experiment is shown. (**C**) Abundance of cells in the MPS gate for each phenotype of interest with or without GM-CSF+G-CSF or GM-CSF+IL6 (n = 4). **P*<.05.

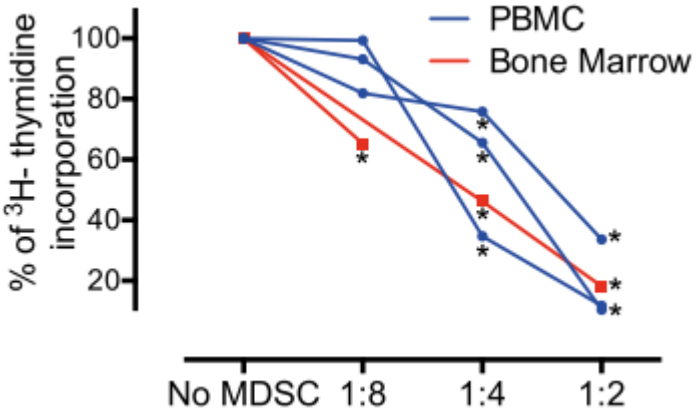

Figure 5: MDSCs derived from PBMC or bone marrow are both suppressive

An allogeneic three-way MLR was performed on MDSCs derived from PBMCs or bone marrows. APCs and T-cells were cultured with no MDSCs and various ratios of MDSCs to T-cells (1:8, 1:4, and 1:2). The inhibition of ^{3}H- thymidine incorporation was evaluated. Results are represented as percentage of inhibition where 100% is the condition without MDSCs. Replicates (3 to 5) wells were performed for each condition. **P*<.05, indicates significant difference when compared to the condition without MDSCs.

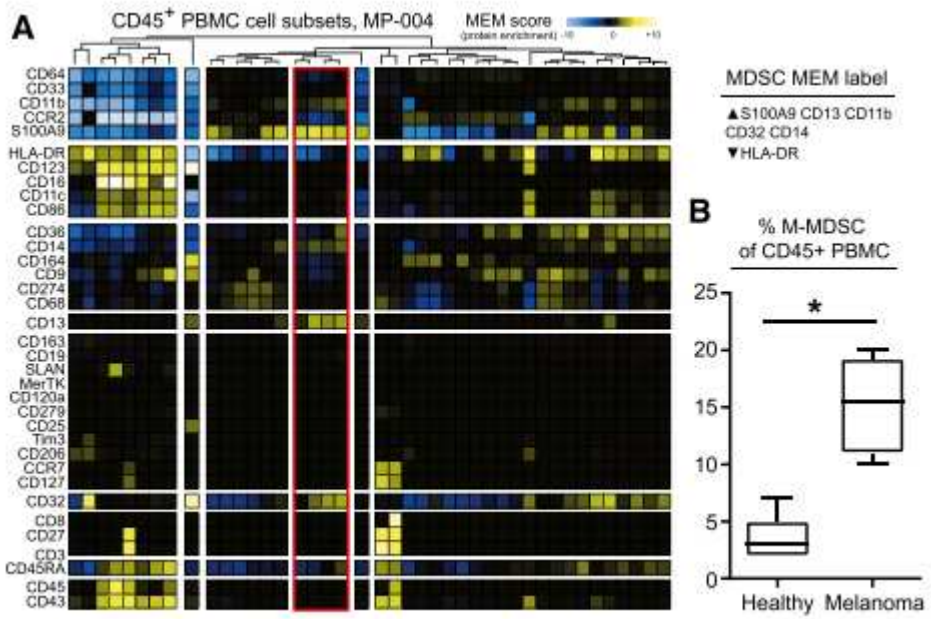

Figure 6: MDSC accumulated in melanoma patient peripheral blood revealed by mass cytometry

(**A**) By mass cytometry analysis, >100,000 $Ir^{pos}CD45^{pos}$ cells were defined on a biaxial plot before viSNE analysis. MPS cells (>20,000 cells) were gated as remaining cells after the exclusion of B- ($CD19^{pos}$), T- ($CD3^{pos}$), and NK- ($CD3^{neg}CD16^{pos}CD45RA^{pos}$) lymphocytes and doublets. Events in the MPS gate were then parsed with SPADE arbitrary restricted to 50 nodes using all clustering markers but CD19 and CD3. After normalization, transformed median expression for each markers and each node are shown on heat map after hierarchical clustering; in red: nodes increased with an increase of $CD14^{pos}$ $S100A9^{pos}$ cells. (**B**) Abundance of $CD14^{pos}$ $S100A9^{pos}$ cells in the MPS gate in PBMC from healthy donor (n=4) and melanoma patients (n=5). *P<.05.